Dhakal *et al. Earth, Planets and Space (2018) 70:189*
https://doi.org/10.1186/s40623-018-0963-9

Earth, Planets and Space

FULL PAPER Open Access

Evidence of strong long-period ground motions of engineering importance for Nankai Trough plate boundary earthquakes: comparison of ground motions of two moderate-magnitude earthquakes

Yadab P. Dhakal*, Wataru Suzuki, Takeshi Kimura, Nobuyuki Morikawa, Takashi Kunugi and Shin Aoi

Abstract

We analyzed strong-motion and broadband recordings of two moderate-magnitude earthquakes that occurred in the Nankai Trough. The first event was the 2004 Mw 6.5 southeast off-Kii peninsula earthquake, an aftershock event inside the Philippine Sea Plate near the Nankai Trough axis. The second event was the 2016 Mw 5.8 southeast off-Mie Prefecture earthquake, an independent event in the rupture area of the 1944 Mw ~ 8 Tonankai earthquake. The centroid depths were 11 and 14 km for the 2004 and 2016 events, respectively. Despite a large difference in the moment magnitude between the two events, the JMA magnitude (Mj) was 6.5 for both the events. We found that the short-period ground motions (e.g., response spectra at periods < 1 s) as well as the much longer-period ground motions (> 20 s) for the 2016 event scaled generally well with the moment magnitude of the event. In contrast, the ground motions from the 2016 event were comparable to those for the larger-moment-magnitude 2004 event at equal distances at periods of about 2–20 s in wide areas and the observed acceleration response spectra at those periods were noticeably underestimated for the 2016 event by the ground motion prediction equation (GMPE) that employs Mw. An examination of the existing subsurface velocity model suggested that the difference in the relative location of the two events with respect to the thick accretionary prism of low seismic velocity most probably caused the comparable amplitude of the seismic waves at those periods. As a result, we posit that the values of Mj are equal for the two events because Mj is estimated using the displacement amplitude of ground motions at periods smaller than about 6 s. On the other hand, GMPE employing Mj generally described the observed data well. The results suggested that the plate boundary earthquakes in the Nankai Trough may excite strong long-period ground motions of engineering importance, and these ground motions appear to be better explained by Mj than by Mw in GMPEs for moderate-magnitude earthquakes in the Nankai Trough subduction zone.

Keywords: Nankai Trough, Plate boundary earthquake, Philippine Sea Plate, Long-period ground motions, Accretionary prism, Tonankai earthquake, Ground motion prediction equations

*Correspondence: ydhakal@bosai.go.jp
National Research Institute for Earth Science and Disaster Resilience, Tsukuba, Japan

Introduction

The Nankai Trough is a prominent geological structure resulting from the continuous subduction of the Philippine Sea Plate beneath the southwest Japan. Large earthquakes with magnitudes around 8 have occurred repeatedly in the region and have caused tremendous damages in southwest Japan (e.g., Ando 1975; Mochizuki and Obana 2003). The Headquarters for Earthquake Research Promotion (HERP), Japan, has estimated probabilities of 70–80% for the next magnitude 8–9 class earthquake to occur within the next 30 years in the Nankai Trough area, based on certain assumptions (HERP 2018). Moderate-magnitude earthquakes are not very frequent in the Nankai Trough compared with those in the Japan Trench area in northeast Japan. On April 1, 2016, an Mw 5.8 earthquake occurred in the coseismic slip area of the 1944 Tonankai earthquake, which was independent of the 2004 southeast off-Kii peninsula earthquake sequence. Ground motions for these earthquakes were recorded by hundreds of strong-motion stations operated by the National Research Institute for Earth Science and Disaster Resilience (NIED). In the present study, we processed and compared the observed ground motion recordings for two moderate-magnitude earthquakes in the Nankai Trough: one having an Mw of 6.5 (an aftershock of the 2004 southeast off-Kii peninsula earthquake) and the other having an Mw of 5.8 (the 2016 southeast off-Mie Prefecture earthquake). According to the revised list of region names for earthquake information by Japan Meteorological Agency (JMA), both the 2004 and 2016 events belong to the same region: Mie-ken Nanto-Oki, which means the southeast off-Mie Prefecture. However, we used the two distinct names for the earthquakes to separate the 2016 event, which presumably occurred as a plate boundary event, from the 2004 earthquake sequence that occurred inside the subducting Philippine Sea Plate as intraslab events. Moreover, the region name for the 2004 event referred to in this paper is consistent with the previous region name (see Availability of data and materials) and the published literature discussed below.

The 2004 Mw 6.5 earthquake occurred as an aftershock of the 2004 off-Kii peninsula earthquake sequence. The mainshock (Mw ~ 7.5) in the sequence occurred on September 5 23:57 JST (UTC + 9 h), while the aftershock analyzed in this study occurred on September 7 08:29 JST. These earthquakes did not overlap with but occurred near the source region of the anticipated megathrust earthquake in the Nankai Trough. As the ground motions from the earthquakes were recorded by the nationwide dense seismic observation network (Okada et al. 2004), the events drew huge attention from the seismological community. The ground motions for the mainshock and the largest foreshock (Mw ~ 7.2) were analyzed by a number of researchers (e.g., Hayakawa et al. 2005; Miyake and Koketsu 2005; Yamada and Iwata 2005; Furumura et al. 2008). Because the earthquakes occurred offshore, about 120 km from inland settlements, the damage done by the earthquakes was limited. On the other hand, significant sloshing of liquid and damage to the gauge pole in a large oil storage tank located on the Kanto Plain, about 400 km from the epicenter of the mainshock, was reported (Hatayama and Zama 2005). Miyake and Koketsu (2005) noted that the 2004 mainshock provided a timely warning of damaging long-period ground motions from future great magnitude Nankai Trough earthquakes. Furumura et al. (2008) showed by computer simulations of long-period ground motions that earthquakes in the Nankai Trough are expected to be the most disastrous as they can produce extraordinarily large and long-duration shakings in the Kanto Plain. However, ground motions from the relatively smaller magnitude aftershock events were not analyzed in detail in previous studies.

The 2004 earthquake sequence was found to consist of shallow intraplate earthquakes that occurred inside the Philippine Sea Plate near the Nankai Trough axis (e.g., Enescu et al. 2005; Sakai et al. 2005). Because these earthquakes occurred inside the subducting Philippine Sea Plate, they are also referred to as intraslab earthquakes. The 2016 Mw 5.8 event, however, which occurred on April 1 11:39 local time, about 85 km closer to land than the 2004 event (Fig. 1), has been suggested to be a plate boundary event (e.g., Wallace et al. 2016; Nakano et al. 2018; Takemura et al. 2018). The 2016 Mw 5.8 event is the largest plate boundary event that occurred in the source region of the 1944 Tonankai earthquake (Mw ~ 8) after its occurrence (Kikuchi et al. 2003; Asano 2018). That the 2016 Mw 5.8 event occurred in the coseismic slip area of the Tonankai earthquake has been interpreted to be an indicator of the ongoing process preparing for the next megathrust earthquake in the Nankai Trough (Nakano et al. 2018). The ground motions for this event were recorded by hundreds of strong-motion stations on land and some tens of ocean bottom seismographs (Kawaguchi et al. 2015). Because the 2016 event and 2004 aftershock event occurred at different locations and their moment magnitudes are different (Table 1), the ground motions recorded at any particular site for the two earthquakes cannot be easily compared. On the other hand, despite the large difference between the moment magnitudes of the two events, the JMA magnitude (Mj) was 6.5 for both (Table 1).

The JMA magnitude and moment magnitude are determined differently. The JMA magnitude is an amplitude-based scale and is determined from the maximum displacement amplitude, high-pass-filtered at a corner

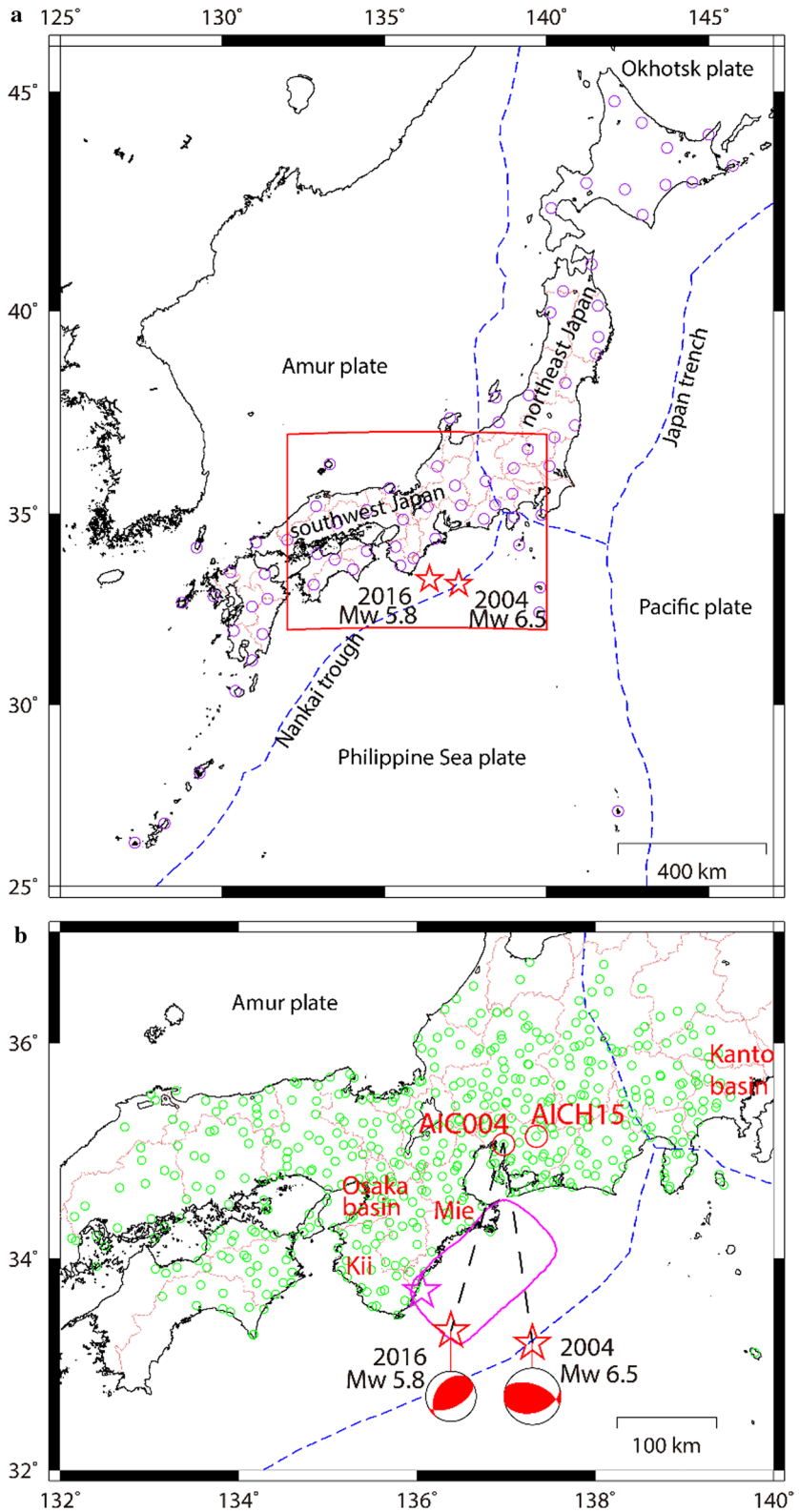

Fig. 1 Index maps. **a** The red stars denote the epicenters of the 2004 Mw 6.5 and 2016 Mw 5.8 earthquakes. The red rectangle denotes the boundary of the enlarged map shown in **b**. The purple circles denote the broadband stations used in the paper. **b** The magenta star and rectangular area denote the epicenter and boundary of the fault model of the 1944 Tonankai earthquake (Kikuchi et al. 2003). Green circles denote the strong-motion stations used in the paper. The black dashed lines denote the surface lines for velocity profiles plotted in Fig. 2

frequency of 6 s (Katsumata 2004). When an earthquake is so small that the magnitude cannot be determined based on the displacement amplitude, the JMA magnitude is determined based on the velocity amplitude using the magnitude formula given by Funasaki and Division (2004). The moment magnitude, however, is determined from the seismic moment by modeling long-period seismic waves. For example, the F-net moment magnitudes are determined by modeling seismic waves in the period range of 20–100 s for moderate events, and 50–200 s for events larger than Mj 7.5 (Kubo et al. 2002). The average JMA magnitude is larger than the moment magnitude by about 0.1 or less in the Mw range of about 5–7 for earthquakes with focal depths smaller than 100 km (Utsu 2002). The reason for the difference between the JMA and moment magnitudes is generally well understood for inland crustal events (e.g., Furumura and Kennett 2001). However, similar phenomena for plate boundary earthquakes have been discussed less in the literature. In this regard, it is important to distinguish the ground motion characteristics of the 2004 and 2016 events for the sake of reliably predicting ground motions of future large plate boundary earthquakes in the Nankai Trough subduction zone.

In this paper, we first describe selection and processing of the data used in the present study. Next, we set up the essential elements for sections that follow by introducing and describing example recordings at two sites common to both events. Thirdly, we compare the peak ground accelerations (PGAs) and peak ground velocities (PGVs) obtained from strong-motion recordings of the two events with reference to the existing ground motion prediction equations (GMPEs). Then, we compare the absolute acceleration response spectra (ARS) of the two events at selected periods between 0.1 and 10 s with reference to GMPEs that employ moment magnitude in their prediction model. Absolute velocity response spectra (AVRS) of the two events at selected periods are then compared with reference to GMPEs that employ JMA magnitude in their prediction model. Following our presentation of the comparisons, we summarize them quantitatively based on an analysis of residuals. We also compare PGVs from broadband recordings at different passbands between 5 and 100 s. Finally, we discuss the implications of our findings for future ground motion predictions for Nankai Trough subduction zone earthquakes.

Data selection and processing

The hypocenter locations and magnitudes of the 2004 and 2016 events used in this paper are listed in Table 1. The hypocenters are taken from the unified JMA hypocenter catalog, and centroid depths and moment magnitudes are taken from F-net moment tensor catalog (Kubo et al. 2002). Figure 1 depicts the epicenter locations for the events. Based on the focal and centroid depths, both events are categorized as intraplate earthquakes. However, in this paper, we treat the 2016 event as a plate boundary event and the 2004 event as an intraslab event based on the published literature, of which some papers were introduced in the previous section. We used the strong-motion data recorded by K-NET and KiK-net and broadband ground motion data recorded by F-net (Okada et al. 2004). The locations of the strong-motion and broadband stations used in this study are depicted in Fig. 1. We selected the strong-motion recordings that contained the arrival of S-waves. The S-wave arrival times were estimated based on a 1D velocity model (JMA 2001, Ueno et al. 2002), and the waveforms were visually inspected to confirm the S-wave arrivals. We also removed records dominated by long-period noises in the target periods by visual inspection of acceleration Fourier spectra, which normally fall off smoothly at longer periods (Brady 1988).

The PGAs, PGVs, and response spectra were calculated from the bandpass-filtered strong-motion seismograms with a cutoff frequency of 0.07 Hz. We computed two types of response spectra: absolute acceleration response spectra and absolute velocity response spectra for a 5% damping ratio. The response spectra were computed following the method of Nigam and Jennings (1969). The values of the PGAs and PGVs were taken as the maximum values of the vector sum (i.e., the square root of the sum of squares) of two horizontal component acceleration and velocity time histories, respectively, over the available time steps, while the response spectra were obtained as the maximum values of the vector sum of two horizontal component response time histories computed for the corresponding periods. The F-net broadband recordings were processed to correct for the effects

Table 1 Source parameters for the earthquakes used in the paper

Origin time (JST)	Epicenter		JMA		NIED	
	Longitude	Latitude	Mj	Depth	Mw	Depth
September 7, 2004, 08:29	137.2928	33.2092	6.5	40	6.5	11
April 1, 2016, 11:39	136.3832	33.3233	6.5	28	5.8	14

of instrumental response, and PGVs were computed at different passband frequencies from the two horizontal component recordings similar to the PGVs of strong-motion recordings.

We used the subsurface velocity model provided by the Japan Seismic Hazard Information Station (J-SHIS 2018) of NIED to extract the depth of the layer beneath the strong-motion sites to correct for the amplification effect of deep sediments on the observed data. These corrections were applied to the observed data for comparison with prediction curves created using the GMPEs. Similarly, the AVS30 (average S-wave velocity in the upper 30 m of the earth beneath the recording station) values derived from the PS-logging information described in Kanno et al. (2006) were employed to correct for shallow soil effects on the observed data. At stations where AVS30 values are not available, geomorphologically derived AVS30 values were used (Matsuoka and Wakamatsu 2008). We also used the Japan integrated velocity structure model (JIVSM) constructed for predicting long-period ground motions in Japan (Koketsu et al. 2012) to supplement the propagation path effects discussed in this study. The JIVSM utilized different kinds of geological and geophysical data sets such as deep borings, reflection and refraction surveys, gravity surveys, microtremor surveys, and earthquake observations, following the standard procedures described in Koketsu et al. (2009, 2012). As an example, the vertical cross sections of the JIVSM along two surface lines are shown in Fig. 2.

Example recordings

In this section, we present recordings from two different sites: AIC004 and AICH15, which are located at similar distances of about 200 km from both the 2004 and 2016 events. See Fig. 1 for the site locations. Site AIC004 is a deep soil site, while AICH15 is a stiff soil site. In fact, the original AIC004 site was moved about 5 m in the horizontal direction, with the old and new locations being separated by a cliff about 2 m high, and the old site being on the cliff side, on October 27, 2004. The AVS20 values at the old and new locations based on 20-m-deep PS-loggings are 274.0 and 278.4 m/s, respectively. We do not think that these small differences in the Vs profiles and the small change in topography would cause large differences at target periods larger than about 1 s. Hence, we consider site AIC004's old and new locations as being the same in the present paper. We present the observations for site AIC004 first. The three-component accelerograms at site AIC004 are plotted in Fig. 3 for both events. The arrival times for the P- and S-waves are also indicated in the figures. Since the K-NET and KiK-net recording systems are triggered based on preset acceleration thresholds, early parts of the P-waves are not available at the site for the 2016 event owing to its smaller P-wave amplitudes. On the other hand, very clear onsets of P- and S-waves can be recognized on all three components for the 2004 event. The PGAs for the 2004 event are about 4–6 times larger than those for the 2016 event. As the original location of site AIC004 was on the 2-m-high cliff, topographic amplification of short-period components of ground motions may have partially contributed to the larger PGAs for the 2004 event. Despite these differences, the coda parts for both events show similar amplitudes.

We present the velocity seismograms obtained by integrating the accelerograms at the AIC004 site for the two events in Fig. 4 to enhance the long-period ground motions. Unlike the accelerograms, the velocity seismograms for the two events have very similar peak amplitudes and both have similar later phases (except for the S-wave parts). The ratio of the PGVs for the two events is about 1.0 for the horizontal components and about 1.5 for the vertical components, the larger values being for the larger-moment-magnitude 2004 event. Having nearly identical PGVs at the AIC004 site does not mean that the PGVs for the two events are similar at equal distances. This is clearly not the case for site AICH15. As explained in the next section, on average, the PGVs for the 2004 event are larger than those for the 2016 event at comparable distances. The Fourier amplitude spectra of the velocity seismograms at site AIC004 are plotted in Fig. 5. The plot clearly shows systematically higher amplitudes at frequencies above about 1 Hz for the 2004 event than those for the 2016 event. By inspecting the S-wave portions of the accelerograms in Fig. 3, it becomes obvious that the large spectral amplitudes at higher frequencies come from the S-wave parts for the 2004 event. In contrast, the amplitudes for the two events are similar at frequencies between 0.1 and 1 Hz (i.e., 1 and 10 s).

The following observations were made at AICH15. AICH15 is a KiK-net site, and PS-logging information is available down to a depth of 120 m at the site. An 8-m-thick top layer with an S-wave velocity of 340 m/s lies over a layer having an S-wave velocity of 900 m/s. The AVS30 value is 663 m/s. The measured S-wave velocity at a depth of 120 m is 2600 m/s. Hence, the site may be considered to be rock with a thin sediment cover. The site's three-component accelerograms are plotted in Fig. 6 for both events. The PGAs for the 2004 event are about 10 times larger than those for the 2016 event. The band-pass-filtered velocity seismograms at periods between 1 and 10 s are compared in Fig. 7. In the figure, surface waves, which arrived noticeably later, dominate the seismograms, and the amplitudes of these phases are comparable for the two events. We show the velocity Fourier

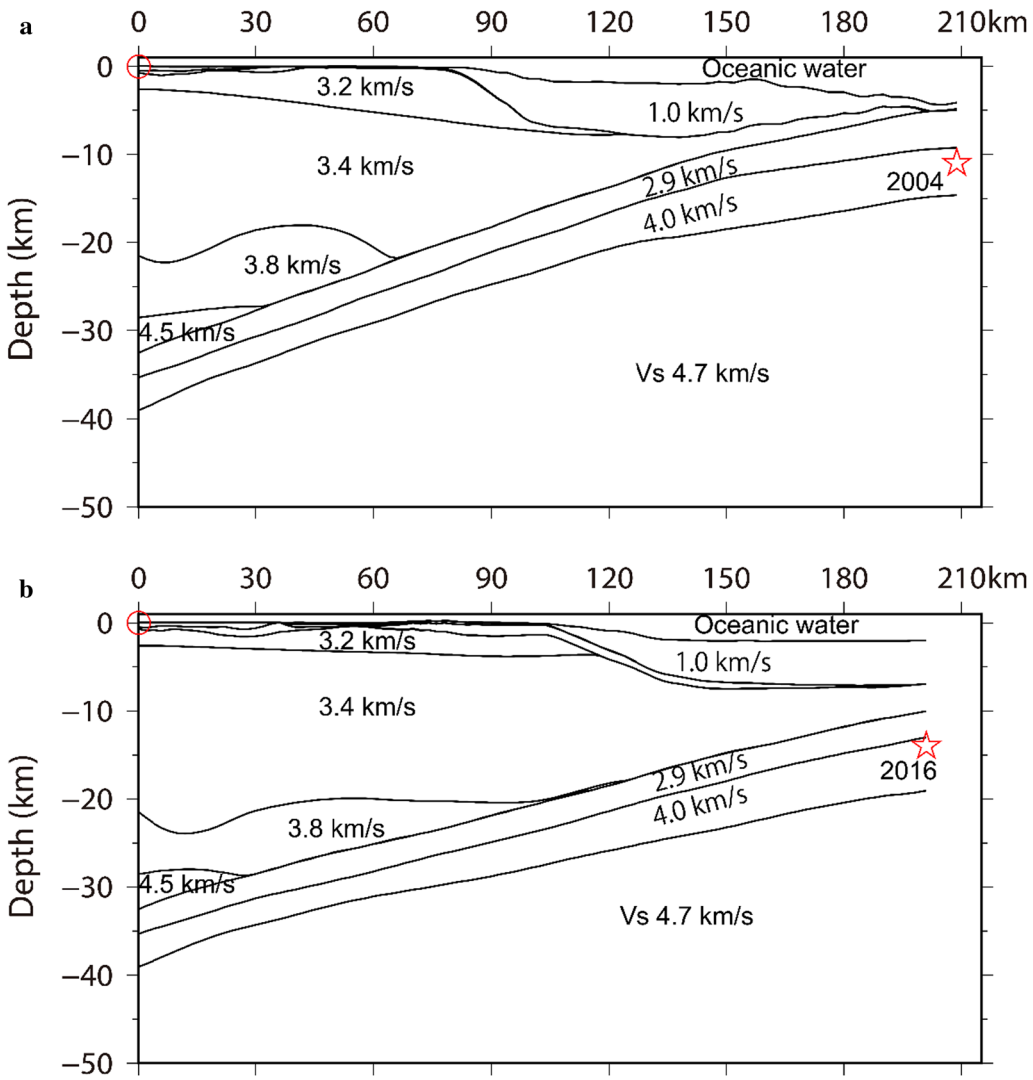

Fig. 2 **a**, **b** Vertical cross sections of the JIVSM along the surface lines joining site AIC004 with the epicenters of the 2004 and 2016 events, respectively. The S-wave velocities in major layers are indicated. The circles and stars denote the location of site AIC004 and the F-net centroid depths of the events, respectively. Note that the vertical and horizontal scales are different

spectra at the site in Fig. 8. Similar to those shown in Fig. 5 for AIC004, the spectral amplitudes are comparable for the two events at periods between about 1 and 10 s, while they are noticeably larger at shorter periods for the 2004 event. The increased spectral amplitudes at periods around 0.15 s (~6.67 Hz), which are seen on the horizontal components for both events, are due to the velocity contrast between the top and lower layers at AICH15, as mentioned above.

The PGAs and PGVs, after adjustments explained in the next section, for the two events are plotted in Fig. 9, and sites AIC004 and AICH15 are indicated on the plots. The plots demonstrate that the difference in the PGVs for the two events is smaller than the corresponding difference in their PGAs. Higher stress drops have been reported to explain the larger PGAs observed for intraslab events in Japan (e.g., Morikawa and Sasatani 2003; Asano et al. 2003). More recently, Baltay et al. (2017) and Oth et al. (2017) showed a clear dependency of ground motion variability on the estimated stress drop. In addition to the difference in the moment magnitude for the two events, the larger PGAs for the 2004 event, which was an intraslab event inside the Philippine Sea Plate, may be interpreted as indicating a higher stress drop.

If we assume that site amplification effects are similar for both events, the similarity between the low-frequency

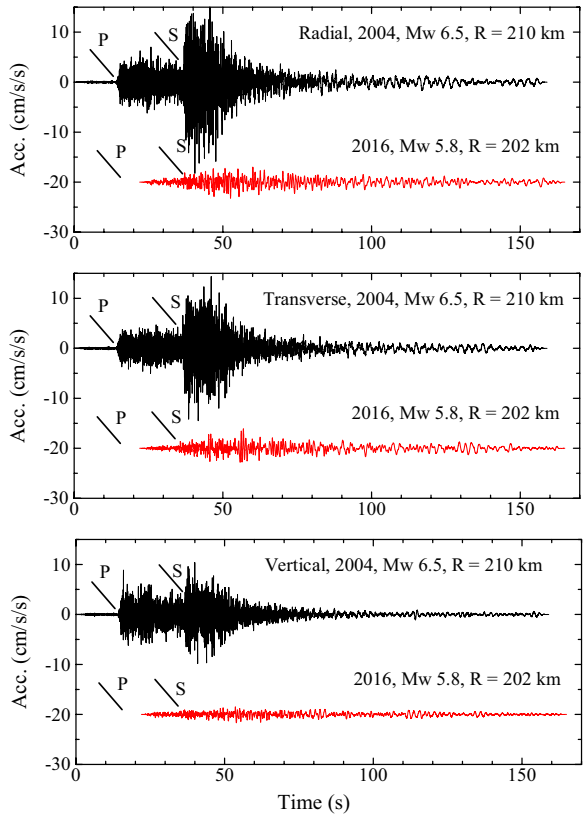

Fig. 3 Plot of radial (upper panel), transverse (middle panel), and vertical (lower panel) component acceleration time histories recorded at site AIC004 (see Fig. 1 for location) for the 2004 (upper trace in each panel) and 2016 (lower trace in each panel) events. The recordings are aligned to match the S-wave arrivals. The arrivals of P- and S-waves are indicated by the letters P and S, respectively. The hypocentral distance (R) is rounded to the nearest whole number. See Fig. 4 for the velocity seismograms at the site and Fig. 9 for a comparison of the adjusted PGAs and PGVs among the sites used

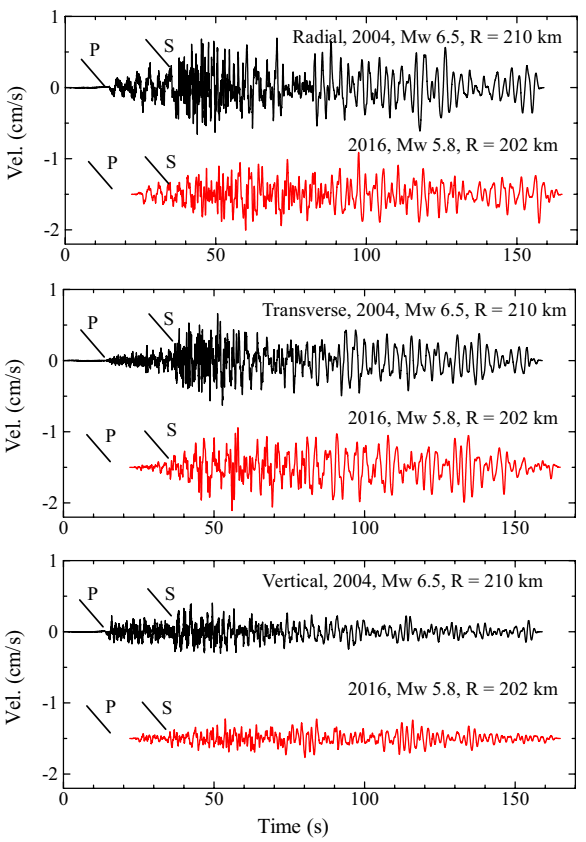

Fig. 4 Plot of radial (upper panel), transverse (middle panel), and vertical (lower panel) component velocity time histories at site AIC004 (see Fig. 1 for location) for the 2004 (upper trace in each panel) and 2016 (lower trace in each panel) events. The recordings are aligned to match the S-wave arrivals. The arrivals of P- and S-waves are indicated by the letters P and S, respectively. See Fig. 3 for the accelerograms at the site and Fig. 9 for a comparison of the adjusted PGAs and PGVs among the sites used

components of the ground motions may be related to earthquake type and path effects. Previous studies have shown relatively smaller PGVs (e.g., Si and Midorikawa 1999) and smaller response spectra at frequencies higher than about 0.1 Hz (e.g., Dhakal et al. 2010; Morikawa and Fujiwara 2013) for inter-plate events than for intraslab events at distances shorter than about 300 km. Since the observations for the 2016 event are contrary to previous results, i.e., the observed values are larger than expected for the moment magnitude of the event, the path effect seems to be a probable reason for the similarity of the spectral amplitudes at frequencies between about 0.1 and 1 Hz (1–10 s). More recently, Uetake (2017) suggested that the existence of thick sedimentary layers above the source region of the shallow earthquake could be the reason for the stronger excitation of long-period surface waves than in the case of similar events lacking thick sedimentary layers above the source. According to the JIVSM, there is a thick (~5 km) low-velocity sedimentary layer ($Vs = 1.0$ km/s) above the centroid location for the 2016 event, while the low-velocity layer is less than 1 km thick above the centroid location for the 2004 event (Fig. 2). Therefore, the effect of thick unconsolidated sediments near the source may be an important contributing factor to the observed large long-period ground motions for the 2016 event.

Comparison of PGAs and PGVs

Morikawa and Fujiwara (2013) updated the database used by Kanno et al. (2006) with additional data and obtained GMPEs for PGAs, PGVs, JMA intensities, and acceleration response spectra between 0.05 and 10 s applicable to different tectonic environments, as well

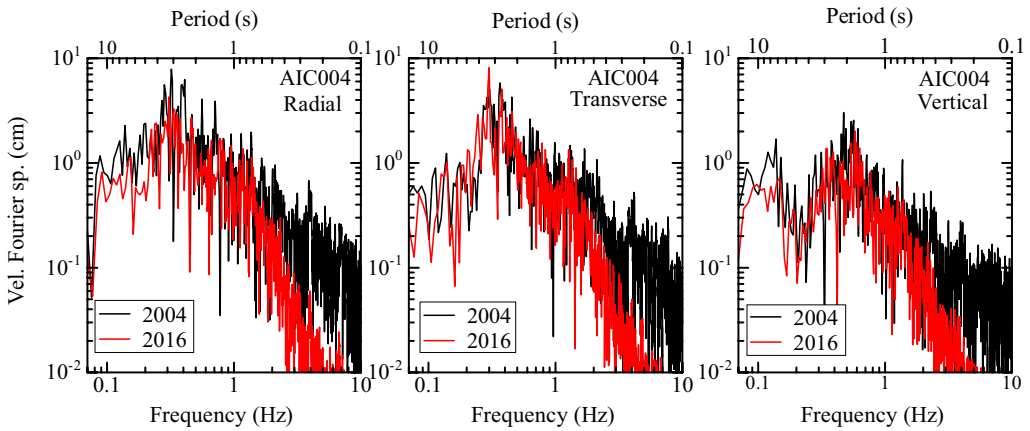

Fig. 5 Plot of radial (left panel), transverse (middle panel), and vertical (right panel) component velocity Fourier amplitude spectra at site AIC004 (see Fig. 1 for location) for the 2004 (black) and 2016 (red) events. See Fig. 4 for the velocity seismograms at the site

as sites located on deep sediments in Japan. Because of their applicability to a wide range of site conditions, we selected the GMPEs in Morikawa and Fujiwara (2013) and adjusted the observed values for amplification due to deep and shallow sediments following the correction terms in the GMPEs. We adopted the hypocentral distance as a measure of the distance between the source fault and the site for use in the GMPEs, considering the moderate size of the earthquakes, and relatively longer distances from the epicenters to the recording stations (>50 km for the 2016 event and >100 km for the 2004 event). The data for the 2004 event were adjusted for the anomalous path effects for west Japan due to the effect of Philippine Sea Plate as described by Morikawa and Fujiwara (2013). These anomalous path effects necessitate general corrections for larger seismic intensity in the fore-arc regions observed during deep-focus events due to effective propagation of high-frequency seismic waves that results from a high Q in the oceanic plates (e.g., Utsu and Okada 1968; Furumura and Kennett 2005). The anomalous path effects considered here are different from those due to unconsolidated sediments in the accretionary prisms discussed later in this study. The adjusted PGAs and PGVs are plotted as functions of hypocentral distance in Fig. 9a, b, respectively. Prediction curves with the ranges of one standard deviation are also plotted. The observed PGAs for the 2016 event (red circles) generally follow the trend of the prediction curve (pink line), and most data lie well within the range of one standard deviation (dashed pink lines), suggesting that the PGAs are typical of those from previous plate boundary events. Unlike the 2016 event, the 2004 event is an intraslab event and the prediction curves plotted are also for intraslab events. The observed PGAs (black circles)

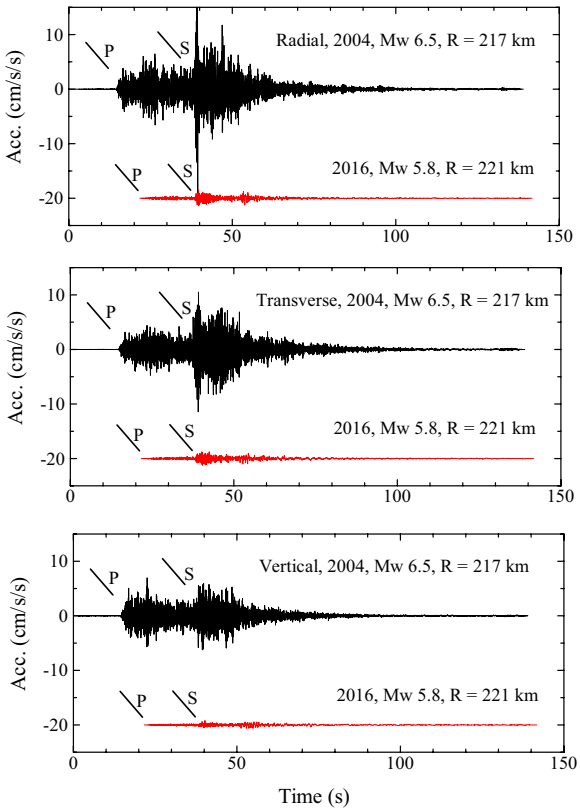

Fig. 6 Plot of radial (upper panel), transverse (middle panel), and vertical (lower panel) component accelerograms at site AICH15 (see Fig. 1 for location) for the 2004 (upper trace in each panel) and 2016 (lower trace in each panel) events. The recordings are aligned to match the S-wave arrivals. The arrivals of P- and S-waves are indicated by the letters P and S, respectively. The hypocentral distance (R) is rounded to the nearest whole number. See Fig. 7 for the bandpass-filtered velocity seismograms at the site and Fig. 9 for a comparison of the adjusted PGAs and PGVs among the sites used

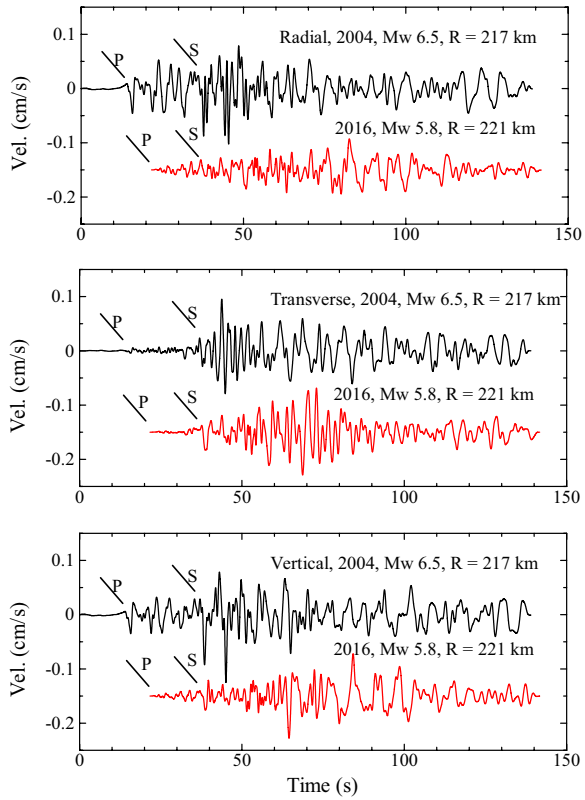

Fig. 7 Plot of radial (upper panel), transverse (middle panel), and vertical (lower panel) component velocity seismograms at site AICH15 (see Fig. 1 for location) for the 2004 (upper trace in each panel) and 2016 (lower trace in each panel) events. The seismograms were bandpass-filtered between 1 and 10 s. The seismograms are aligned to match the S-wave arrivals. The arrivals of P- and S-waves are indicated by the letters P and S, respectively. See Fig. 6 for the accelerograms at the site and Fig. 9 for a comparison of the adjusted PGAs and PGVs among the sites used

for the 2004 event are noticeably underestimated by the GMPEs, with many data points more than one standard deviation above the curve (dashed gray lines). This suggests that the radiation of short-period ground motions was stronger for this event than the median values for previous intraslab events. The PGVs also generally follow a trend similar to that for the PGAs for the 2016 event, while the PGVs for the 2004 event are better explained by the prediction curves, unlike the PGAs. In summary, the PGAs and PGVs for the 2004 event are generally larger than those for the 2016 event, and while the PGAs for the 2016 event are consistent with the prediction curves, the PGA values for the 2004 event suggest event-specific radiation.

To get a rough idea on the strength of high-frequency radiation, we estimated the approximate values of the corner frequencies for the two events using the S-wave recordings at two selected F-net stations located at rock sites. An additional file is provided that deals with the estimation of the corner frequencies for the two events (see Additional file 1). We found that the corner frequencies for the 2004 event are higher than or similar to those for the 2016 event. Given the similar corner frequencies for the two events, the stress drop for the 2004 event is expected to be much larger because the seismic moment of the 2004 event is larger by a factor of about 12 than that for the 2016 event (Brune 1970, 1971). Stress drop may be considered as one of the parameters that control the strength of high-frequency radiation (Boore 1983). In fact, as mentioned above, the observed PGAs were clearly underestimated by the GMPEs for the 2004 event, while the prediction was reasonable for the 2016 event. Together, these observations may indicate that the 2004 event was a higher stress drop event.

Comparison of ARS

Figure 10 shows a comparison of the acceleration response spectra for the two events at periods of 0.1, 0.5, 1, 2, 5, and 10 s. Similar to the modifications described in the previous section, the values were adjusted for site amplification effects for the two events and anomalous path effects for the 2004 event using the equations of Morikawa and Fujiwara (2013). It can be seen that the values at 0.1 and 0.5 s generally follow the trend of the prediction curves for the 2016 event, while the values are clearly underestimated at these periods for the 2004 event. The values for the 2004 event are clearly larger than those for the 2016 event at comparable distances. In contrast, it can be seen that the response values for the two events are similar at many sites between 1 and 10 s, and the median prediction curve for the 2016 event clearly underestimates the observed values at periods of about 2–10 s at most sites and at distances beyond about 100 km. It is noteworthy that the data at distances smaller than 100 km generally conform with the prediction curves at periods smaller than about 5 s. This may be explained by the peak amplitudes being produced mostly by body waves at short distances, and the effect of path-amplified surface waves not being so strong. However, the observed values for 10 s are clearly underestimated at small distances (< 100 km) by the prediction curves (bottom right panel in Fig. 10). In general, the systematically larger values than those implied by the GMPEs, especially at distances beyond 100 km, may indicate propagation path effects for the 2016 event. We discuss this further in later sections.

Comparison of AVRS

Unlike the moment magnitude, the JMA magnitude for both the 2004 and 2016 events is 6.5. Considering the faster estimation of the JMA magnitude, Dhakal et al.

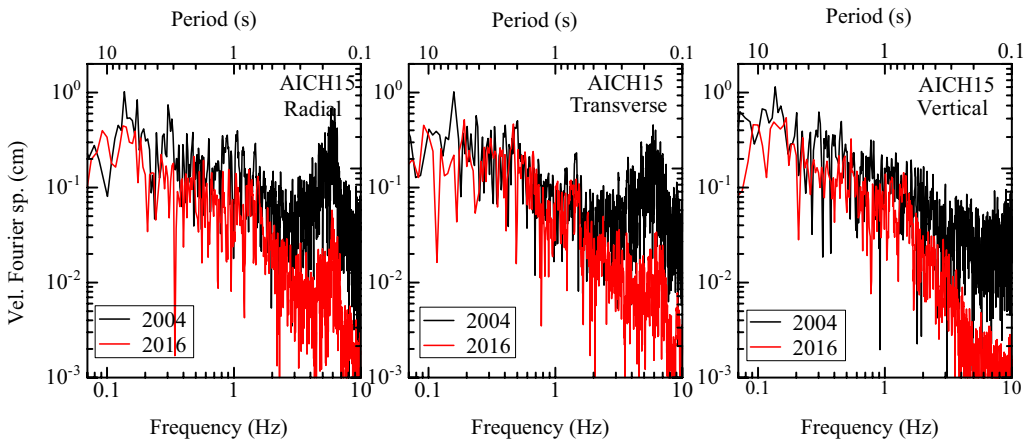

Fig. 8 Plot of radial (left panel), transverse (middle panel), and vertical (right panel) component velocity Fourier amplitude spectra at the AICH15 site (see Fig. 1 for location) for the 2004 (black curve) and 2016 (red curve) events. See Fig. 7 for the bandpass-filtered velocity seismograms and Fig. 6 for the accelerograms at the site

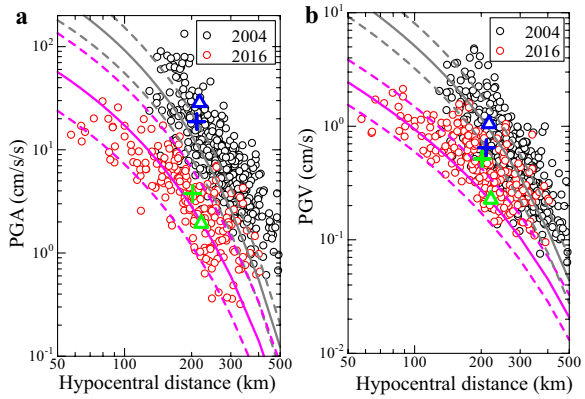

Fig. 9 Comparison of peak ground accelerations (PGAs), **a**, and peak ground velocities (PGVs), **b**, observed for the 2004 (black circles) and 2016 (red circles) events. The blue and green crosses denote the values at site AIC004 for the 2004 and 2016 events, respectively. Similarly, the blue and green triangles denote the values at site AICH15 for the two events. The gray and pink solid lines denote the median predictions using the GMPEs (Morikawa and Fujiwara 2013) for the 2004 and 2016 events, respectively. The dashed gray and pink lines show a range of one standard deviation for the corresponding events. The observed values were adjusted for site amplification effects for both events, and the anomalous path effect due to the subducting Philippine Sea Plate for the 2004 event. Note that the correction for the anomalous path effect due to the subducting plate is required only for recordings from events located inside the oceanic plates

(2015) constructed GMPEs for absolute velocity response spectra at periods between 1 and 10 s from the viewpoint of early warning of earthquake long-period ground motions using the JMA magnitude, hypocentral distance, and site correction terms. They used events having focal depths shallower than 50 km and treated all events identically despite their different tectonic settings. Site parameters, namely AVS30 and depth of deep sediments, were employed to obtain the site correction coefficients. The site parameters were identical to those employed by Morikawa and Fujiwara (2013). The AVRS, relative velocity response spectra, and pseudo-velocity response spectra are identical at the peak response period and differ gradually at longer or shorter periods (Dhakal et al. 2014). In this section, we compare the observed AVRS for the two events with reference to the GMPEs of Dhakal et al. (2015).

The observed AVRS values were adjusted using the same site parameters (AVS30 and depth of sediments) as used to predict the ARS in the previous section and are plotted in Fig. 11 at periods of 1, 2, 3, 5, 7, and 10 s. Because of the identical JMA magnitudes, a single median prediction curve with a range of one standard deviation is drawn at each period for both events. As described in the previous section for the ARS, the observed values for the two events overlap considerably at all periods between 1 and 10 s and at distances beyond 100 km. At distances smaller than 100 km, the observed AVRS are generally overpredicted by the GMPEs at periods smaller than 7 s. On the other hand, the observed values are generally well described by the GMPEs for both events at longer distances, suggesting that the observed data are not systematically different from those for past shallow-focus events with identical JMA magnitudes.

We show the spatial distribution of the observed AVRS at a period of 10 s for the 2004 and 2016 events in Fig. 12. At this period, the GMPEs for the ARS clearly underestimated the observed values for the 2016 event as shown

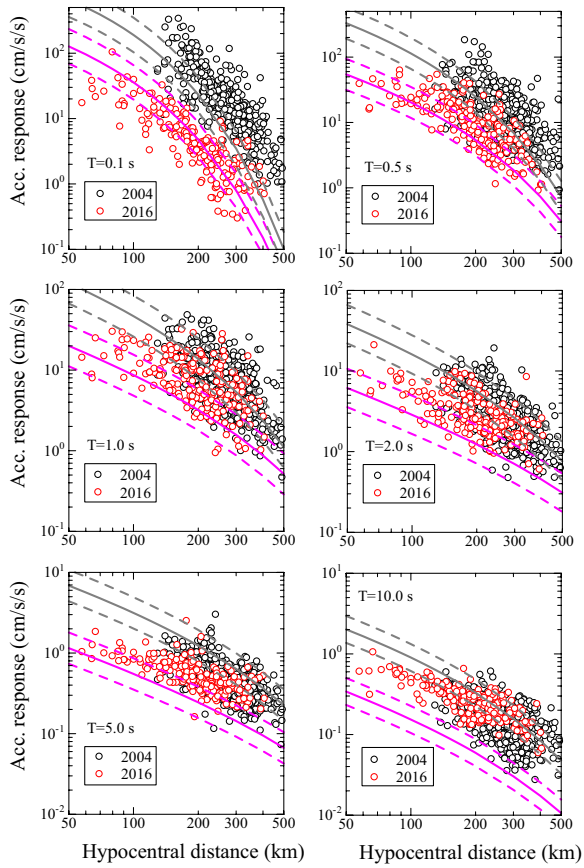

Fig. 10 Comparison of the observed acceleration response spectra (ARS) between the 2004 (black circles) and 2016 (red circles) events at selected periods. The gray and pink solid lines denote the median predictions using the GMPEs (Morikawa and Fujiwara 2013) for the 2004 and 2016 events, respectively. The dashed gray and pink lines show a range of one standard deviation for the corresponding events. The observed values were adjusted for site amplification effects for both events, and the anomalous path effect due to the subducting Philippine Sea Plate for the 2004 event

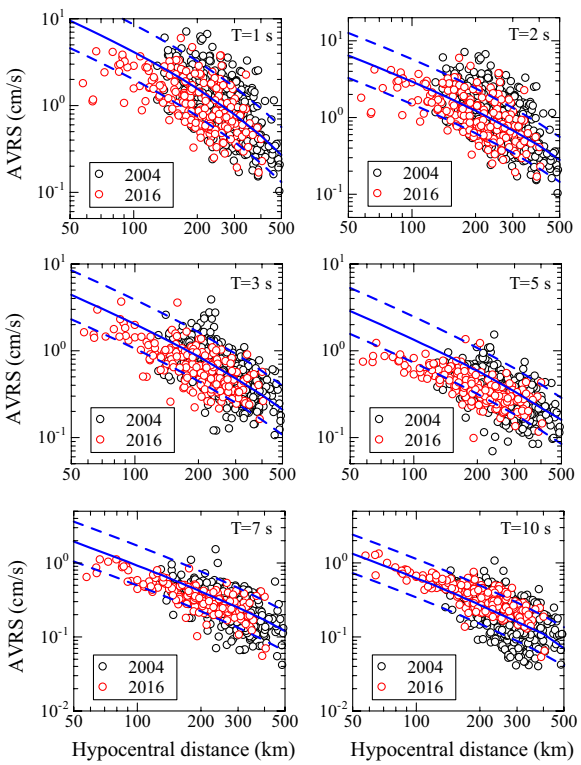

Fig. 11 Comparison of the observed absolute velocity response spectra (AVRS) for the 2004 (black circles) and 2016 (red circles) events at selected periods. The solid blue lines denote the median predictions using the GMPEs for AVRS (Dhakal et al. 2015) for Mj = 6.5. The dashed blue lines indicate a range of one standard deviation for the GMPEs

in Fig. 10 (bottom right panel), while the observed values for the 2004 and 2016 events are comparable at equal distances. Figure 12 shows circles with radii of 100–400 km at intervals of 100 km. Their centers lie at the epicenters of the two events. The spatial distributions of the data illustrate that the strong-motion recordings for the 2004 event come from more stations over a relatively wider area than those for the 2016 event. This is because the K-NET and KiK-net system is triggered based on preset acceleration thresholds, and the 2004 event generated much stronger short-period ground motions, such as PGAs, than the 2016 event.

Despite the difference in the number of recordings, the general distribution pattern is identical at a period of 10 s for the two events. Large response values can be seen at sites located in sedimentary basins such as the Osaka basin for both events. At equal distances, such as between radii of 200 and 300 km, the observed values and their distribution are similar for the two events. This suggests that seismic waves with a period of about 10 s were similarly excited and/or transmitted from areas close to the sources. We discuss the similarity of ground motions at longer periods further in later sections.

Quantitative comparisons

To augment the qualitative comparisons described above, we computed mean residuals and standard deviations with respect to the GMPEs to summarize the comparisons numerically. Because the difference between the two events is obvious at short periods, two statistical parameters (the mean and standard deviation of the residuals) are computed for selected periods between 1 and 10 s. The data were divided into three groups based on hypocentral distances: those smaller than 100 km, those between 100 and 200 km, and those larger than

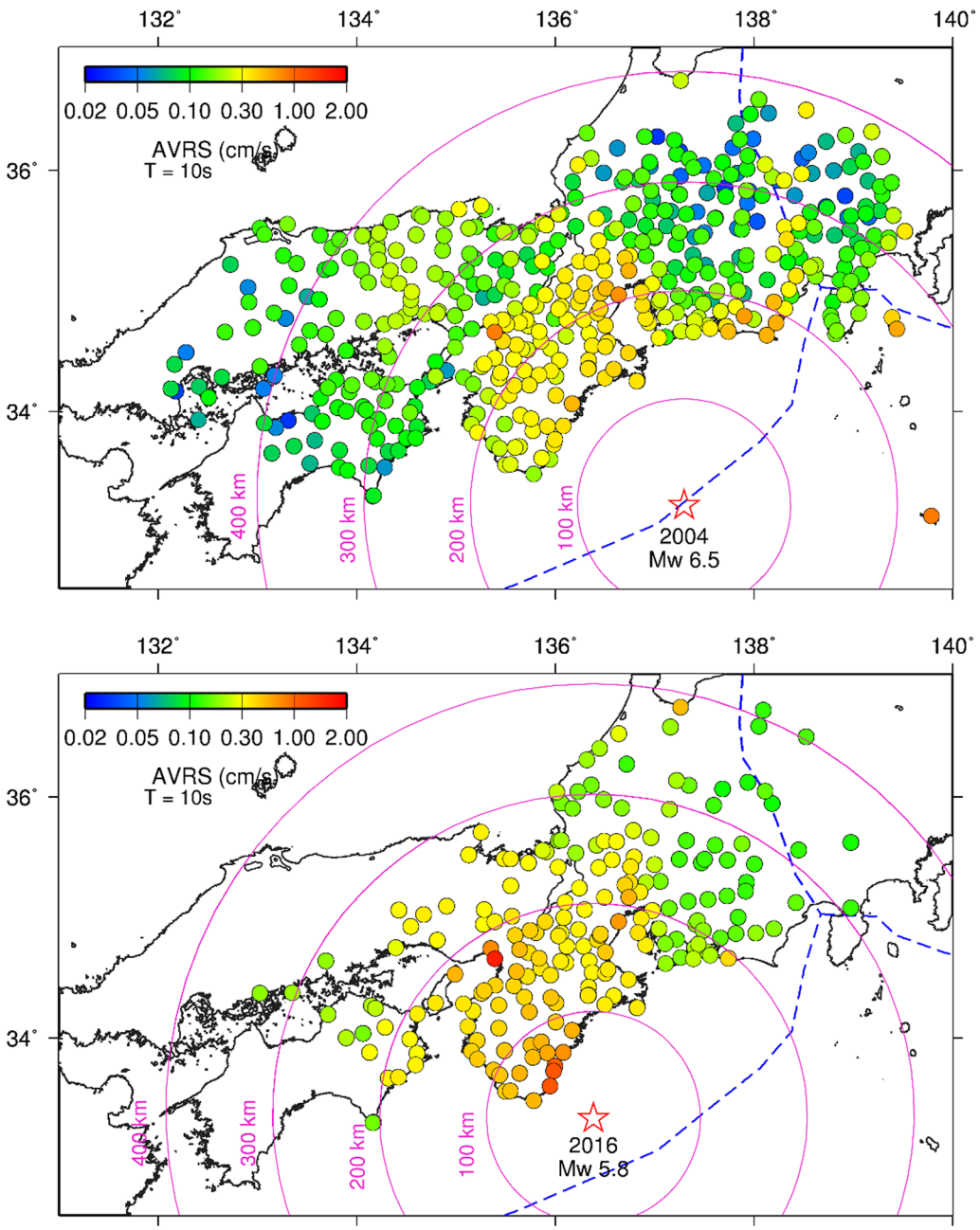

Fig. 12 Spatial distribution of AVRS at the period of 10 s for the 2004 Mw 6.5 event (upper panel) and 2016 Mw 5.8 event (lower panel). Circles are drawn for radii of 100, 200, 300, and 400 km with the epicenters as the centers of the circles

200 km. The mean residuals and standard deviations were computed at periods of 1, 2, 5, 7, and 10 s. The mean residuals are computed for each group of data from the logarithmic differences between the observed values and those predicted using the GMPEs for the ARS and AVRS described above. Positive values indicate underprediction (i.e., the observed values are larger than the predictions), on average, over the range of analysis, while negative values indicate the opposite. Similarly, the standard deviations are computed from the logarithmic differences of the observed and predicted values as root-mean-square residuals in each group of data.

The computed mean residuals and standard deviations are plotted in Figs. 13, 14, respectively. The mean residuals for the 2004 event for distances between 100 and 200 km (Fig. 13a) and longer than 200 km (Fig. 13b)

are negative using both GMPEs. The absolute values are slightly smaller at distances longer than 200 km. In contrast to the 2004 event, the mean residuals for the 2016 event (Fig. 13c, d) using the GMPEs of Morikawa and Fujiwara (2013) are positive, and the values are larger at distances greater than 200 km than at distances between 100 and 200 km. The mean residuals in Fig. 13a indicate that the median predictions (Morikawa and Fujiwara 2013) are larger than the observed values by factors of about 1.5–2.0 for the 2004 event at distances between 100 and 200 km. On the other hand, the mean residuals for the 2016 event for the corresponding distances and periods (Fig. 13c) indicate that the observed values are larger than the median predictions by factors of about 2.0–3.5, the largest value being for a period of 10 s. The observed data deviate more at distances beyond 200 km and are larger than the median predictions by factors of about 2.5–4.5 for the 2016 event (Fig. 13d). The mean residuals using the GMPEs of Dhakal et al. (2015) show consistent

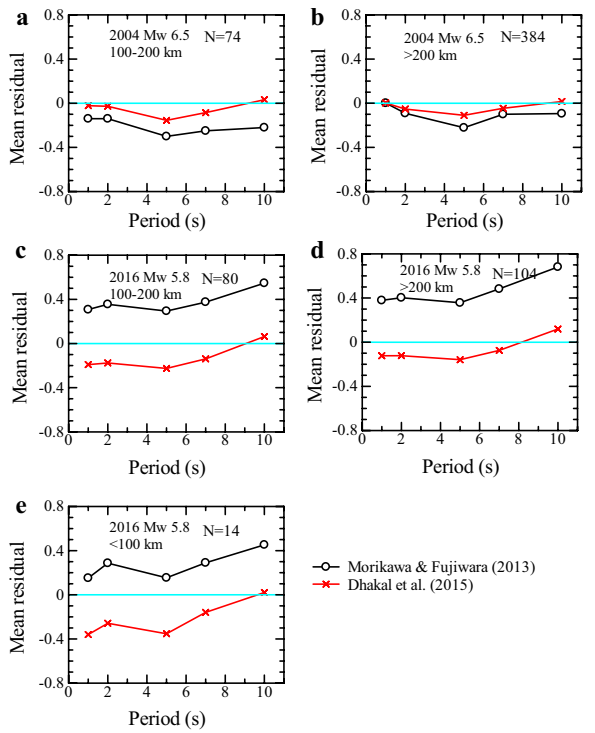

Fig. 13 Mean residuals as a function of period and distance for the 2004 Mw 6.5 and 2016 Mw 5.8 events. The black line with circles and red line with diagonal crosses denote the mean residuals on a base-10 log-scale with respect to the GMPEs of Morikawa and Fujiwara (2013) and Dhakal et al. (2015), respectively. **a** 2004 event for distances between 100 and 200 km. **b** 2004 event for distances larger than 200 km. **c** 2016 event for distances between 100 and 200 km. **d** 2016 event for distances larger than 200 km. **e** 2016 event for distances smaller than 100 km. The number of data points used in the analysis is denoted by the letter N in each panel

values (mostly negative mean residuals) for both the 2004 and 2016 events, and the absolute values are smaller than those from Morikawa and Fujiwara (2013). The absolute mean residuals for distances smaller than 100 km for the 2016 event (Fig. 13e) are comparable for the two GMPEs except for the 10-s period. Its mean residual is approximately zero using the GMPEs of Dhakal et al. (2015), but is about 0.4 using the GMPEs of Morikawa and Fujiwara (2013). However, there are only 14 data points in the group closer than 100 km, so the results presented in Fig. 10e may not be conclusive. See Fig. 13 for the number of data points in each group as delineated above. The standard deviations plotted in Fig. 14 correspond well with the results presented in Fig. 13; the larger the mean residual, the larger the standard deviation. The standard deviations are generally smaller using the GMPEs of Dhakal et al. (2015) for both the 2004 and 2016 events, except for the group of data closer than 100 km from the epicenter. The standard deviations are considerably smaller for the 2016 event at periods of 7 and 10 s for data at distances larger than 100 km using the GMPEs of Dhakal et al. (2015). In general, the standard deviations obtained in the present study for the 2004 event are either similar to or somewhat larger than the tabulated standard deviations of Morikawa and Fujiwara (2013) using their equations. The standard deviations for the 2016 event using their GMPEs, however, are two to three times larger than the tabulated values, especially at periods of 7–10 s. In summary, the larger absolute mean residuals and standard deviations for the 2016 event based on the GMPEs of Morikawa and Fujiwara (2013) suggest that the 2016 event differed systematically from the average characteristics of past earthquakes of similar moment magnitudes, while the data at corresponding periods from that event generally follow the GMPEs of Dhakal et al. (2015).

Comparison of PGVs from broadband recordings

In the previous section, we described the results of some statistical analyses of the residuals between the observed strong-motion data and median predictions determined using GMPEs. The strong-motion data were recorded by K-NET and KiK-net and were mostly for distances within 400 km of the epicenters (for example, see Figs. 10 and 12). The K-NET and KiK-net recordings have limitations at much longer periods such as 20–100 s due to either a low signal-to-noise ratio or a limited duration for moderate earthquakes. The F-net waveform data, on the other hand, are continuous and are recorded in a low-noise system and environment. As a result, ground motions at much longer periods, such as 50–100 s, and for much longer distances, at which strong-motion stations

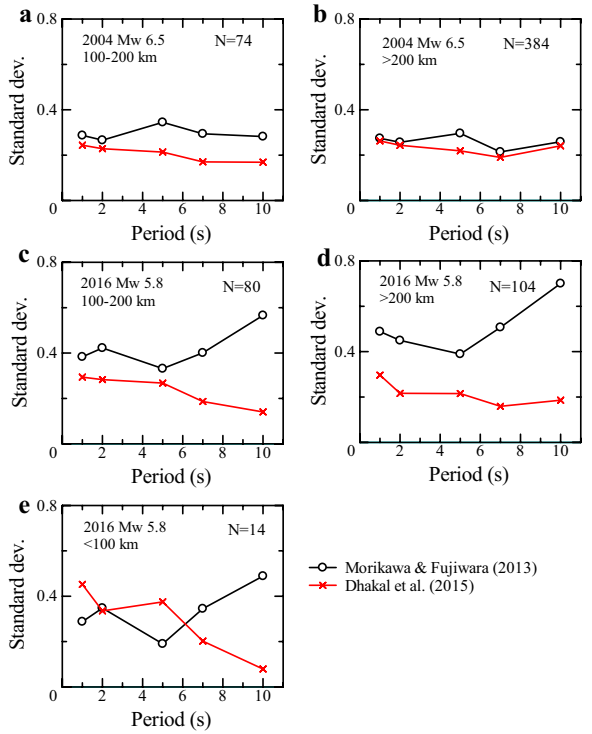

Fig. 14 Standard deviations as a function of period and distance for the 2004 Mw 6.5 and 2016 Mw 5.8 events. The black line with circles and red line with diagonal crosses denote the standard deviations on a base-10 log-scale with respect to the GMPEs in Morikawa and Fujiwara (2013) and Dhakal et al. (2015), respectively. **a** 2004 event for distances between 100 and 200 km. **b** 2004 event for distances larger than 200 km. **c** 2016 event for distances between 100 and 200 km. **d** 2016 event for distances larger than 200 km. **e** 2016 event for distances smaller than 100 km. The number of data points used in the analysis is denoted by the letter N in each panel

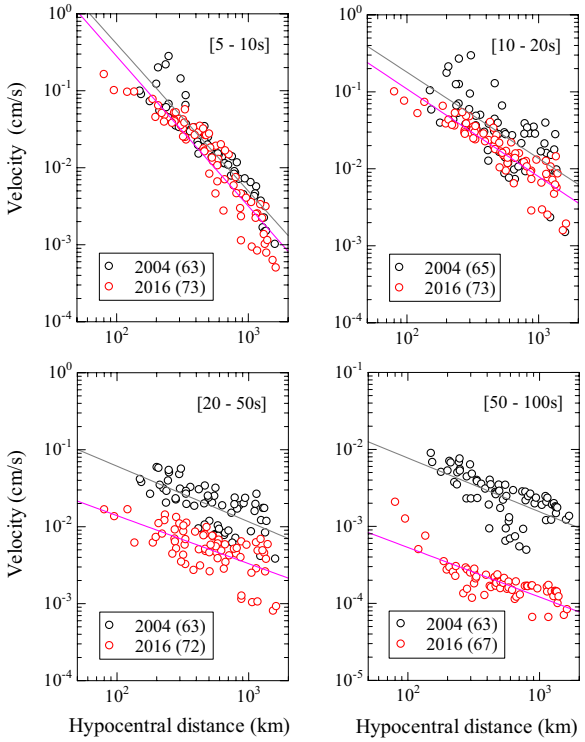

Fig. 15 Comparison of the PGVs at different passbands for the 2004 (black circles) and 2016 (red circles) events. The passbands are indicated near the top right corner of each plot inside the square brackets. The number of recordings for each event is indicated in parentheses with the data legends. Note that the number of recordings may differ between the passbands due to the presence of noise on the recordings. The gray and pink lines denote the linear best fit to the relationship between the PGVs and hypocentral distances for the 2004 and 2016 events, respectively, calculated using the least square method

were not triggered, can be evaluated using the F-net recordings.

In this section, we compare the PGVs for the 2004 and 2016 events at different passbands using the broadband ground motion data recorded by F-net all over Japan. For some stations, the PGVs were obtained from velocity-type strong-motion sensors collocated at F-net broadband stations to avoid the effect of amplitude saturation (Fukuyama et al. 1996). The PGVs were obtained at four different passbands: 5–10 s, 10–20 s, 20–50 s, and 50–100 s using second-order Butterworth filtering. The locations of the F-net stations used in this study are plotted in Fig. 1a, and the PGVs at the above-mentioned passband frequencies are plotted in Fig. 15. Similar to the results presented in the previous sections, the PGVs for the 5–10 s passband are similar at equal distances for the two events except at some sites. In the 10–20-s passband, differences between the two events start to appear, but the values still overlap at many sites. However, the PGVs at passbands of 20–50 s and 50–100 s clearly separate into two groups of values.

The PGVs at different passbands are regressed separately with respect to the hypocentral distances for the corresponding events using the linear least square method, and the fitted lines are drawn in Fig. 15. The fitted lines clearly show different slopes for the different passbands, becoming gentler as the period increases. These results support the longer-period ground motions decaying slowly with distance. The difference between the fitted lines for the two events increases as the period increases at equal distances, while the difference remains generally constant for a given passband regardless of distance. As evidenced from the plot for the longest periods (50–100 s) analyzed in this study, we found that on average the ratio (~13) of the fitted values is similar to the ratio of the seismic moments (6.0E + 18 Nm to 4.9E + 17 NM ~ 12), estimated by F-net (NIED) for the two events.

Site amplification effects may be neglected at periods over 5 s at the F-net stations because the stations are set up inside tunnels constructed on stiff or hard rock. Both events were reverse fault events with similar dip amounts, and the station coverage is almost identical for the two events. There were more than 60 recordings covering all of Japan for each event. Therefore, the similarities at periods of 5–20 s for these two events that had a significantly large difference in moment magnitude may be attributed to factors closely related to path effects.

Discussion

We compared the observed peak ground motions for the 2004 Mw 6.5 off-Kii peninsula and 2016 Mw 5.8 southeast off-Mie Prefecture earthquakes. The comparisons were complimented with GMPEs based on past earthquake recordings. Based on these comparisons, the two earthquakes are nearly identical in terms of their peak ground motions at periods of about 2–20 s, but their short-period (smaller than about 2 s) and much longer-period (larger than 20 s) peak ground motions are clearly different. Obviously, their tectonic locations and moment magnitudes are different based on results published by many researchers. The Mw for the 2016 event, estimated by the Global CMT project (e.g., Ekström et al. 2012), is 5.9, which is identical to that estimated for the 2016 event by Asano (2018) using the empirical Green's function method (Irikura 1986; Irikura et al. 1997) based mostly on ocean bottom recordings, while the corresponding value from the F-net moment tensor catalog is 5.8. Similarly, the Mw for the 2004 event is 6.6 in the Global CMT catalog, while it is 6.5 in the F-net moment tensor catalog. Such differences in the value of the moment magnitude arise from differences between the data sets, crustal and subsurface velocity models, mathematical approximations, and other factors used in the simulations (e.g., Kubo et al. 2002). For example, moment magnitudes differing by up to 0.5 units have been reported for the same moderate-magnitude events under thick sediments during the 2012 Ferrara seismic sequence in northeast Italy. These discrepancies were caused mainly by differences in the velocity models employed in the inversions (e.g., Malagnini and Munafò 2017). More recently, Takemura et al. (2018) estimated the moment magnitude of the 2016 event in the Nankai Trough using the 3D Green's function computed by 3D FDM employing a realistic 3D subsurface velocity model that includes both the unconsolidated soft sediments and subducting oceanic plates. Their estimated moment magnitude is 5.6 for the 2016 event, compared to its 5.8 F-net and 5.9 GCMT catalog magnitudes. If we took the 5.6 value into consideration in the GMPEs, the observed data for the 2016 event would be further underestimated by the GMPEs presented in Figs. 9, 10. This means that shallow plate boundary events in the Nankai Trough produce significantly large ground motions at periods of about 1–10 s in relation to the GMPEs of Morikawa and Fujiwara (2013). One of the reasons for the differences between the GMPEs (Morikawa and Fujiwara 2013) and the data, particularly for the 2016 event, is that the GMPEs for plate boundary-type events were constructed using mostly plate boundary events in northeast Japan due to the lack of corresponding records in the Nankai Trough subduction zone.

Furumura et al. (2008) performed 3D simulations of long-period ground motions for the 1944 Tonankai earthquake using the source model proposed by Yamanaka (2004) and a detailed 3D velocity model reconstructed by Tanaka et al. (2006) comprising the subducting Philippine Sea Plate and the overlying sedimentary layer in the accretionary wedge. The simulations of the Tonankai earthquake produced about ten times larger peak ground displacements and velocity response spectra at periods larger than 2 s in the Kanto Plain, located about 400 km from the epicentral area, than those for the observed Mw ~ 7.5 mainshock event of the 2004 off-Kii peninsula earthquakes. The large difference was largely due to the greater moment magnitude of the Tonankai earthquake (Mw 8.1). In contrast, in the present study, the 2016 event is smaller than the 2004 event by 0.7 moment magnitude units, but the observed ground motions at periods of about 2–20 s are as strong as those for the 2004 event. These observations may suggest that the subsurface velocity structure in the Nankai Trough subduction zone is favorable for producing much stronger long-period ground motions for plate boundary events than for intraplate events inside the Philippine Sea Plate due to its proximity to overlying unconsolidated sediments. More recently, Uetake (2017) compared ground motions for two shallow crustal events having identical JMA magnitudes (Mj 6.7), similar moment magnitudes (Mw 6.2 and 6.3), similar focal depths, similar focal mechanisms, and similar source-to-target-site distances in central Japan. The subsurface velocity structures were clearly different near the source regions of the two events. One event, which originated beneath a relatively thick, low-velocity sedimentary layer, excited surface waves of larger amplitudes with a dominant period of about 5 s. These waves propagated into the Kanto Plain, which further amplified and trapped the waves to produce large, long-duration shaking. By complementing the observations with simulations, Uetake (2017) confirmed the effects of the subsurface velocities in the source regions on long-period ground motions. The vertical cross sections of the JIVSM plotted in Fig. 2 show that the thickness of low-velocity sediments is much larger in the source region of the 2016 Mw 5.8 event than in the source region of the 2004 Mw

6.5 event. The 2004 event also generated significant long-period shaking, but the comparable peak amplitudes of ground motion at periods of 2–20 s for the smaller-moment-magnitude 2016 event are most likely due to differences in the subsurface velocity structures near the source regions of the two earthquakes.

An analysis of seismic moments from many shallow-focus, inland, and plate boundary earthquakes by Takemura (1990) suggested that the excitation of somewhat longer-period surface waves near the sources for shallow-focus and inland earthquakes could be the reason for the larger JMA magnitudes for these earthquakes even when their seismic moments are similar to ordinary plate boundary earthquakes in northeast Japan. The larger Mj values for crustal events away from subduction zones in western Japan are posited to be related to the efficient propagation of Lg-type waves in the region (Furumura and Kennett 2001). Seismic wave propagations for the 2016 event may also have been compounded by wave-guide effects due to the subducting Philippine Sea Plate in the offshore region, and Lg-type wave conversion and transmission through the inland crustal structure in southwest Japan (Furumura et al. 2014). Together, all these effects contributed to the JMA magnitude being larger by 0.7 magnitude units than its F-net catalog Mw value of 5.8.

Dhakal et al. (2015) employed Mj and Mw separately in identical ground motion prediction models for events having Mw > 6.5 and found that inter-event errors were significantly smaller using Mj than those using Mw at periods between 1 and 10 s. The results were obtained for events including a large proportion of data from plate boundary events with focal depths smaller than 50 km in northeast Japan as well as inland earthquakes. On average, the JMA magnitude was larger than the Mw for events having Mw values smaller than about 7 in their data set, and for some events, the difference was 0.4 or larger. It has now become apparent that the GMPEs by Dhakal et al. (2015) described the observed response spectra of the 2016 Mw 5.8 event well at periods between about 2 and 10 s without correction for propagation path effects caused by either thick sediments or surface waves generated near the source, while GMPEs employing Mw appear to be insufficient without correction for propagation path effects in the Nankai Trough, especially for events whose JMA and moment magnitudes are significantly different. The GMPEs of Dhakal et al. (2015) were constructed from an earthquake early warning viewpoint. Therefore, their GMPEs should be used with caution for other purposes such as the seismic hazard analysis. Nonetheless, the findings of this study clearly indicate the necessity of considering propagation path effects in the GMPEs for seismic hazard evaluation of long-period ground motions in the Nankai Trough. Moreover, evaluating the long-period ground motions of future Nankai Trough plate boundary earthquakes will be greatly assisted by further validation of the available velocity models against observed data for moderate-magnitude earthquakes.

Conclusions

We analyzed strong-motion and broadband ground motion data for the 2004 Mw 6.5 southeast off-Kii peninsula earthquake, an offshore aftershock event that occurred inside the Philippine Sea Plate near the Nankai Trough axis. We also analyzed similar data for the 2016 Mw 5.8 southeast off-Mie Prefecture earthquake, an independent offshore event in the source area of the 1944 Tonankai earthquake. Despite a large difference in the moment magnitudes for the two events, their magnitudes in the JMA magnitude scale were identical, both being 6.5. We found that the PGAs and ARS at periods smaller than about 0.5 s were noticeably underestimated by the GMPEs for the 2004 event, while the ARS at longer periods were generally well explained. In contrast, the PGAs and ARS at periods smaller than about 1 s were generally explained well by the GMPEs for the 2016 event, while the ARS at periods of about 2–10 s were significantly underestimated, especially at distances larger than about 100 km. We found that the ground motions for the 2016 event (Mw 5.8) were comparable to those for the larger-moment-magnitude 2004 event (Mw 6.5) at equal distances for periods of engineering importance of about 2–20 s over wide areas. We checked the existing subsurface velocity model, which suggested that the difference in the relative location of the two events, particularly with respect to the presence of a thick accretionary prism of low seismic velocity in the Nankai Trough, might have caused the difference between the two events in their excitation of seismic waves with periods of 2–20 s. Interestingly, it was found that the observed ARS are generally consistent with the GMPEs at distances shorter than about 100 km for the 2016 event. These observations suggested that the large response spectra at periods of about 2–10 s for the 2016 event at larger distances are not due to source effects. Moreover, GMPEs employing Mj generally described the observed AVRS well at corresponding periods for both events. These results suggest that the intensity of long-period ground motions at periods of about 2–10 s may be better represented by Mj than by Mw in GMPEs for shallow and moderate earthquakes in the Nankai Trough subduction zone, unless some adjustments are made in Mw-based GMPEs to account for propagation path effects due to the accretionary wedge in the Nankai Trough.

Additional file

Additional file 1. Estimation of corner frequencies.

Abbreviations

CMT: centroid moment tensor; FDM: finite difference method; F-net: full-range seismograph network; GMPE: ground motion prediction equation; JMA: Japan Meteorological Agency; JIVSM: Japan integrated velocity structure model; J-SHIS: Japan Seismic Hazard Information Station; KiK-net: Kiban Kyoshin network; K-NET: Kyoshin network; Mj: JMA magnitude; Mw: moment magnitude; NIED: National Research Institute for Earth Science and Disaster Resilience; PGA: peak ground acceleration; PGV: peak ground velocity; Vs: S-wave velocity; 1D: one-dimensional; 3D: three-dimensional.

Authors' contributions

YPD analyzed the data, organized discussions, and drafted the manuscript. WS, TK, NM, TK, and SA provided insightful comments. All authors took part in revising the manuscript. All authors read and approved the final manuscript.

Acknowledgements

We would like to thank the Japan Meteorological Agency for providing us with hypocenter information for the earthquakes used in this study. We also used moment magnitudes from Global CMT project. We would like to thank Wessel and Smith (1998) for providing us with Generic Mapping Tools, which were used to make some figures in this paper. We would also like to thank the Headquarter for Earthquake Research Promotion, Japan, for providing us with the subsurface velocity model (JIVSM). We are thankful to editor, Dr. Kimiyuki Asano, reviewer, Dr. Dino Bindi, and an anonymous reviewer for their constructive comments which helped us significantly improve the manuscript.

Competing interests

The authors declare that they have no competing interests.

Availability of data and materials

The strong-motion (K-NET and KiK-net) and broadband (F-net) recordings used in this study were downloaded from the Web sites: http://www.kyoshin.bosai.go.jp/ and http://www.fnet.bosai.go.jp/freesia/top.php?LANG=en, respectively. The J-SHIS subsurface velocity models and JIVSM used in this study were downloaded from the Web sites: http://www.j-shis.bosai.go.jp/en/ and https://www.jishin.go.jp/evaluation/seismic_hazard_map/lpshm/12_choshuki_dat/, respectively. The hypocenter location and JMA magnitudes were taken from the Web site: https://www.data.jma.go.jp/svd/eqev/data/bulletin/hypo_e.html. The moment magnitudes and centroid depths were taken from the Web site: http://www.fnet.bosai.go.jp/event/joho.php?LANG=en. The region names of earthquakes may be found at https://www.jma.go.jp/jma/press/0609/20b/20060920chiiki.html, in Japanese. For other specific information such as the list of recordings used in the study, contact authors for data requests.

Funding

This study was supported by "Advanced Earthquake and Tsunami Forecasting Technologies Project" of NIED.

Publisher's Note

Received: 16 July 2018 Accepted: 26 November 2018
Published online: 06 December 2018

References

Ando M (1975) Source mechanisms and tectonic significance of historical earthquakes along the Nankai trough, Japan. Tectonophysics 27:119–140. https://doi.org/10.1016/0040-1951(75)90102-X

Asano K (2018) Source modeling of an Mw 5.9 earthquake in the Nankai trough, southwest Japan, using offshore and onshore strong-motion waveform records. Bull Seismol Soc Am 108:1231–1239. https://doi.org/10.1785/0120170357

Asano K, Iwata T, Irikura K (2003) Source characteristics of shallow intraslab earthquakes derived from strong-motion simulations. Earth Planets Space 55:e5–e8. https://doi.org/10.1186/BF03351744

Baltay AS, Hanks TC, Abrahamson NA (2017) Uncertainty, variability, and earthquake physics in ground-motion prediction equations. Bull Seismol Soc Am 107:1754–1772. https://doi.org/10.1785/0120160164

Boore DM (1983) Stochastic simulation of high-frequency ground motions based on seismological models of the radiated spectra. Bull Seismol Soc Am 73:1865–1894

Brady AG (1988) Processing of digitally-recorded seismic strong-motion accelerations. In: Proceedings of the second workshop on processing of seismic strong motion records (part 2), pp 255–263

Brune JN (1970) Tectonic stress and the spectra of seismic shear waves from earthquakes. J Geophys Res 75:4997–5009. https://doi.org/10.1029/JB075i026p04997

Brune JN (1971) Correction. J Geophys Res 76:5002. https://doi.org/10.1029/JB076i020p05002

Dhakal YP, Takai N, Sasatani T (2010) Empirical analysis of path effects on prediction equations of pseudo-velocity response spectra in northern Japan. Earthq Eng Struct Dyn 39:443–461. https://doi.org/10.1002/eqe.952

Dhakal YP, Kunugi T, Suzuki W, Aoi S (2014) Comprehensive analyses of absolute, relative, and pseudo relative velocity response spectra (1–10 s) in terms of ground motion prediction equations. In: Proceedings of the 14th Japan earthquake engineering symposium, Chiba, Japan, pp 604–613

Dhakal YP, Suzuki W, Kunugi T, Aoi S (2015) Ground motion prediction equations for absolute velocity response spectra (1–10s) in Japan for earthquake early warning. J Jpn Assoc Earthq Eng 15(6):91–111. https://doi.org/10.5610/jaee.15.6_91

Ekström G, Nettles M, Dziewonski AM (2012) The Global CMT project 2004–2010: centroid-moment tensors for 13,017 earthquakes. Phys Earth Planet Inter 200–201:1–9. https://doi.org/10.1016/j.pepi.2012.04.002

Enescu B, Mori J, Ohmi S (2005) Double-difference relocations of the 2004 off the Kii peninsula earthquakes. Earth Planets Space 57:357–362. https://doi.org/10.1186/BF03352576

Fukuyama E, Ishida M, Hori S, Sekiguchi S, Watada S (1996) Broadband seismic observation conducted under the FREESIA project. Rep Natl Res Inst Earth Sci Disaster Prev 57:23–31 **(in Japanese with English abstract)**

Funasaki J, Division Earthquake Prediction Information (2004) Revision of the JMA velocity magnitude. Q J Seismol 67:11–20 **(in Japanese with English abstract)**

Furumura T, Kennett BLN (2001) Variations in regional phase propagation in the Area around Japan. Bull Seismol Soc Am 91:667–682. https://doi.org/10.1785/0120000270

Furumura T, Kennett BLN (2005) Subduction zone guided waves and the heterogeneity structure of the subducted plate: intensity anomalies in northern Japan. J Geophys Res 110:B10302. https://doi.org/10.1029/2004JB003486

Furumura T, Hayakawa T, Nakamura M, Koketsu K, Baba T (2008) Development of long-period ground motions from the Nankai trough, Japan, earthquakes: observations and computer simulation of the 1944 Tonankai (Mw 8.1) and the 2004 SE off-Kii peninsula (Mw 7.4) earthquakes. Pure Appl Geophys 165:585–607. https://doi.org/10.1007/s00024-008-0318-8

Furumura T, Hong TK, Kennett BLN (2014) Lg wave propagation in the area around Japan: observations and simulations. Progr Earth Planet Sci 1:10. https://doi.org/10.1186/2197-4284-1-10

Hatayama K, Zama S (2005) Sloshing of liquid in oil storage tanks and long-period strong ground motions due to 2004 M 7-class earthquakes southeast off the Kii Peninsula. Rep Natl Res Inst Fire Disaster 99:52–67 **(in Japanese with English abstract)**

Hayakawa T, Furumura T, Yamanaka Y (2005) Simulation of strong ground motions caused by the 2004 off the Kii peninsula earthquakes. Earth Planets Space 57:191–196. https://doi.org/10.1186/BF03351814

Headquarters for Earthquake Research Promotion (HERP) (2018) Evaluation of occurrence potentials of subduction-zone earthquakes. https://www.jishin.go.jp/main/index-e.html. Last accessed in July 2018 (**in Japanese**)

Irikura K (1986) Prediction of strong acceleration motions using empirical Green's function. In: Proceedings of the 7th Japan earthquake engineering symposium, Tokyo, Japan, pp 151–156

Irikura K, Kagawa T, Sekiguchi H (1997) Revision of the empirical Green's function method by Irikura (1986). Prog Abstr Seismol Soc Japan, 2(B25) (**in Japanese**)

Japan Seismic Hazard Information Station (J-SHIS) (2018) http://www.j-shis.bosai.go.jp/en/. Last Accessed in March 12, 2018

Kanno T, Narita A, Morikawa N, Fujiwara H, Fukushima Y (2006) A new attenuation relation for strong ground motion in Japan based on recorded data. Bull Seismol Soc Am 96:879–897. https://doi.org/10.1785/0120050138

Katsumata A (2004) Revision of the JMA displacement magnitude. Q J Seismol 67:1–10 **(in Japanese with English abstract)**

Kawaguchi K, Kaneko S, Nishida T, Komine T (2015) Construction of the DONET real-time seafloor observatory for earthquakes and tsunami monitoring. In: Favali P, Beranzoli L, De Santis A (eds) Seafloor observatories a new vision of the earth from the abyss, pp 211–228. https://doi.org/10.1007/978-3-642-11374-1_10

Kikuchi M, Nakamura M, Yoshikawa K (2003) Source rupture process of the 1944 Tonankai earthquake and the 1945 Mikawa earthquake derived from low-gain seismograms. Earth Planets Space 55:159–172. https://doi.org/10.1186/BF03351745

Koketsu K, Miyake H, Afnimar Tanaka Y (2009) A proposal for a standard procedure of modeling 3-D velocity structures and its application to the Tokyo metropolitan area, Japan. Tectonophysics 472:290–300. https://doi.org/10.1016/j.tecto.2008.05.037

Koketsu K, Miyake H, Suzuki H (2012) Japan integrated velocity structure model version 1. In: Proceedings of 15th world conference on earthquake engineering, Lisbon, Portugal

Kubo A, Fukuyama E, Kawai H, Nonomura K (2002) NIED seismic moment tensor catalogue for regional earthquakes around Japan: quality test and application. Tectonophysics 356:23–48. https://doi.org/10.1016/S0040-1951(02)00375-X

Malagnini L, Munafò I (2017) M_ws of seismic sources under thick sediments. Bull Seismol Soc Am 107:1413–1420. https://doi.org/10.1785/0120160243

Matsuoka M, Wakamatsu K (2008) Site amplification capability map based on the 7.5-arc second Japan engineering geomorphologic classification map. National Institute of Advanced Industrial Science and Technology, Intellectual property management, No. H20PRO-936 (**in Japanese**)

Miyake H, Koketsu K (2005) Long-period ground motions from a large offshore earthquake: the case of the 2004 off the Kii peninsula earthquake, Japan. Earth Planets Space 57:203–207. https://doi.org/10.1186/BF03351816

Mochizuki K, Obana K (2003) Seismic activities along the Nankai trough. Bull Earthq Res Inst 78:185–195

Morikawa N, Fujiwara H (2013) A new ground motion prediction equation for Japan applicable up to M9 mega-earthquake. J Disaster Res 8:878–888. https://doi.org/10.20965/jdr.2013.p0878

Morikawa N, Sasatani T (2003) Source spectral characteristics of two large intra-slab earthquakes along the southern Kurile-Hokkaido arc. Phys Earth Planet Inter 137:67–80. https://doi.org/10.1016/S0031-9201(03)00008-6

Nakano M, Hyodo M, Nakanishi A, Yamashita M, Hori T, Kamiya S, Suzuki K, Tonegawa T, Kodaira S, Takahashi N, Kaneda Y (2018) The 2016 Mw 5.9 earthquake off the southeastern coast of Mie Prefecture as an indicator of preparatory processes of the next Nankai Trough megathrust earthquake. Prog Earth Planet Sci 5:30. https://doi.org/10.1186/s40645-018-0188-3

Nigam NC, Jennings PC (1969) Calculation of response spectra from strong motion earthquake records. Bull Seismol Soc Am 59:909–922

Okada Y, Kasahara K, Hori S, Obara K, Sekiguchi S, Fujiwara H, Yamamoto A (2004) Recent progress of seismic observation networks in Japan —Hi-net, F-net, K-NET and KiK-net—. Earth Planets Space 56:xv–xxviii. https://doi.org/10.1186/BF03353076

Oth AH, Miyake H, Bindi D (2017) On the relation of earthquake stress drop and ground motion variability. J Geophys Res Solid Earth 122:5474–5492. https://doi.org/10.1002/2017JB014026

Sakai S, Yamada T, Shinohara M, Hagiwara H, Kanazawa T, Obana K, Kodaira S, Kaneda Y (2005) Urgent aftershock observation of the 2004 off the Kii Peninsula earthquake using ocean bottom seismometers. Earth Planets Space 57:363–368. https://doi.org/10.1186/BF03352577

Si H, Midorikawa S (1999) New attenuation relations for peak ground acceleration and velocity considering effects of fault type and site condition. J Struct Constr Eng Trans AIJ 523:63–70. https://doi.org/10.3130/aijs.64.63_2 **(in Japanese with English abstract)**

Takemura M (1990) Magnitude-seismic moment relations for the shallow earthquakes in and around Japan. Zisin 43:257–265. https://doi.org/10.4294/zisin1948.43.2_257 **(in Japanese with English abstract)**

Takemura S, Kimura T, Saito T, Kubo H, Shiomi K (2018) Moment tensor inversion of the 2016 southeast offshore Mie earthquake in the Tonankai region using a three-dimensional velocity structure model: effects of the accretionary prism and subducting oceanic plate. Earth Planets Space 70:50. https://doi.org/10.1186/s40623-018-0819-3

Tanaka Y, Miyake H, Koketsu K, Furumura T, Hayakawa T, Baba T, Suzuki H, Masuda T (2006) The DaiDaiToku integrated model of the velocity structure beneath the Tokyo metropolitan area (2). Abst Jpn Geosci Union Meet, pp S116–P014

Ueno H, Hatakeyama S, Aketagawa T, Funasaki J, Hamada N (2002) Improvement of hypocenter determination procedures in the Japan Meteorological Agency. Q J Seismol 65:123–134 **(in Japanese)**

Uetake T (2017) Effects of subsurface structures of source regions on long-period ground motions observed in the Tokyo Bay area, Japan. Earth Planets Space 69:71. https://doi.org/10.1186/s40623-017-0655-x

Utsu T (2002) Relationships between magnitude scales. In: Lee W, Kanamori H, Jennings P, Kisslinger C (eds) International handbook of earthquake and engineering seismology 81A, pp 733–746

Utsu T, Okada H (1968) Anomalies in seismic wave velocity and attenuation associated with a deep earthquake zone (II). J Fac Sci, Hokkaido Univ Jpn, Ser. VII 3(2):65–84

Wallace LM, Araki E, Saffer D, Wang X, Roesner A, Kopf A, Nakanishi A, Power W, Kobayashi R, Kinoshita C, Toczko S, Kimura T, Machida Y, Carr S (2016) Near-field observations of an offshore Mw 6.0 earthquake from an integrated seafloor and subseafloor monitoring network at the Nankai trough, southwest Japan. J Geophys Res Solid Earth 121:8338–8351. https://doi.org/10.1002/2016JB013417

Wessel P, Smith WHF (1998) New, improved version of generic mapping tools released. EOS Trans AGU 79:579. https://doi.org/10.1029/98EO00426

Yamada N, Iwata T (2005) Long-period ground motion simulation in the Kinki area during the MJ 7.1 foreshock of the 2004 off the Kii peninsula earthquakes. Earth Planets Space 57:197–202. https://doi.org/10.1186/BF03351815

Yamanaka Y (2004) Source process of the 1944 Tonankai and the 1945 Mikawa earthquake. Chikyu Mon 305:739–745